Pure & Appl. Chem., Vol. 65, No. 12, pp. 2481–2500, 1993.
Printed in Great Britain.

Characterization of metallic and ceramic high-temperature materials for energy systems by means of atomic spectroscopy

Hubertus Nickel
Research Centre Jülich, Institute for Reactor Materials and Technical University, Aachen D-5170 Jülich 1, Germany

Abstract
In nuclear and non-nuclear energy systems high temperature alloys and ceramics are used. The special physical requirements require that these materials be characterized very carefully using modern physio-chemical methods. The problems associated with surface analysis, coatings, oxide layers and the growth mechanisms of protecting layers are discussed especially with respect to characterization and analysis. Techniques such as optical spectroscopy, X-ray fluoresence, SIMS, and others are considered with regard to the problems.

1. INTRODUCTION

1.1 Primary energy demand and possible resources

The availability of sufficient, economically produced energy is a key factor in the development of modern societies. The global energy consumption is today about 12 billion tce. According to a comprehensive study this energy consumption will rise to about 28 billion tce by the year 2030 (so-called low scenario)[1], world population increasing from more than 5 billion to more than 8 billion over the same period. To put these figures into perspective to today, mankind consumed less primary energy since the invention of the steam engine about 300 years ago than it will probably consume within the next 30 years. The energy carriers utilized today on a large technical scale are therefore not capable of satisfying such a demend for energy, if nuclear energy is excluded. The possible sources of energy to be mentioned are:

a) fossil resources (coal, mineral oil, natural gas, etc.);

b) so-called renewable energy sources (solar, hydropower, wind, geothermal, tidal as well as combustible plants and organic wastes), and

c) nuclear energy sources (i.e. the nuclear power stations available today, advanced reactor concepts and fusion reactors).

At the present time, coal is the major fuel used to produce electricity. It is well known that in the case of coal, as with any other fossil fuel, particular attention must be given to the carbon dioxide (CO_2) problem. For example, the combustion of 1000 billion tce fossil energy resources up to the year 2030, which seems to be almost indispensible in view of the above-mentioned scenario, would double the CO_2 content in the atmosphere. Carbon dioxide emitted represents a type of waste which nature will not tolerate in the long run without serious consequences. Experts are therefore warning of the possible consequences of steady CO_2 increase; in particular, it is known that changes in the ratio of the CO_2 concentration to oxygen can influence plant and animal enzymes[2].

The well known Club of Rome has in a new report directed their studies primarily to the world energy demand and the global warming[3]. To delay and buffer earth-heating and eventually to bring it to a halt the fundamental need is to reduce the CO_2 emission by massively reducing the combustion of fossil fuels. The 1988 Toronto Conference of scientists suggested that it would be necessary to reduce CO_2 emission by some 20% by 2005. A worldwide campaign of energy conversation and efficiency (e.g. combined cycles) as well as the development of soft energy is on the way. Looking to the above-mentioned long time energy prospects the following perspective can be summarized:

- Oil is too precious: Measures should be instituted gradually to conserve this vital resource as a feed-stock for the petro-chemical industry.

- Coal is too polluting: there still is plenty, but it seems as if it is becoming too dangerous to use because of global warming, unless the technological progress makes it possible to considerably limit its negative effects.

- Renewables are insufficient: According to estimates, renewable energy sources will not even cover 10% of the overall demand for energy by the turn of the millenium despite all efforts. This is due to the development of costs, and, as far as solar energy is concerned, a solution must be found to the transport and storage problems[4].

- Fusion is too far in the future: Nuclear fusion has not yet passed the threshold to its physical realization, although some experimental progress has been achieved especially in the past few years. A commercial utilization of nuclear fusion with significant contributions to the energy supply is not to be expected within the next 50 years.

- Nuclear fission energy seems to be the only possibility: Today nuclear energy sources are used primarily for producing electricity in light water reactors (LWRs) as pressurized or boiling water reactor types (PWR or BWR) in highly developed countries. Advanced reactor systems such as the liquid metal fast breeder reactor (LMFBR) and the helium-cooled high temperature (HTR) have been promoted in several countries. Recent years have shown that the contribution to energy supply that can be furnished by nuclear energy is influenced neither by the uranium and thorium reserves available nor by technical aspects, but rather depends on how the problem of institutional and social acceptance is solved. The prime objectives for better acceptance is to find a solution for the final disposal of radioactive materials and to reduce the probability of damaging events like in Chernobyl in future nuclear power stations. For the final waste disposal many activities are underway in the industrialized countries. The best solution seems to be the storage of radioactive waste at great depths in a stable, water insoluble geological formations; this concept cannot be a problem for the foreseeable future nor even for posterity. In the reactor development particular progress has been made in the field of light-water reactors where safety is ensured by a large number of engineered safeguards. Further research and design activities are underway to construct, new so-called evolved or innovated 'Advanced Light-Water Reactor' (ALWR) concepts with passive system functions, as LWRs of the next generation. Another reactor system is the helium-cooled high temperature reactor with its favourable safety characteristics. It has been demonstrated that the HTR can be used at high temperature niveau not only for electricity production but also for process heat applications.

Considering the specified amounts of energy available for the three energy resource categories (fossil, renewable, nuclear) it is evident that nuclear energy sources cannot be abandoned even in the near future and taking the 'low scenario' as a basis.

Irrespective of the systems and the status of the energy producing systems in general and of the nuclear reactor development lines in particular, the availability, qualification and development of materials are crucial.

This paper concentrates on some requirements and the status of development and characterization of high temperature metallic and ceramic materials for nuclear and nonnuclear energy systems.

2. CHARACTERIZATION METHODS FOR SURFACE ANALYSIS

High temperature alloys based on iron and nickel and structural ceramics are used in different technical applications. The main requirements for the metallic materials are directed to the mechanical properties, e.g. creep rupture strength and the fatigue behaviour. Very often these alloys are exposed to corrosive atmospheres at high temperatures, so that in addition to the mechanical properties, the oxidation and corrosion mechanisms and the stability of protective scales are of high importance. The stability of an alloy attack by a corrosive atmosphere is dependent on the properties of the oxide scales formed on the surface. For determining the oxidation kinetics and the corrosion mechanisms of the high temperature alloys at different temperatures, times and gas compositions, different analytical methods are necessary. Bauer[5] and Müller[6] discussed and tabulated the methods for characterizing solid state surfaces, oxidation and corrosive layers, protective coatings and thin coatings. As an example, Table 1 lists the coating properties and methods of characterization. Experiences with these methods are described in the literature. In our own investigations the composition and morphology of the surface layers were examined by metallography or ceramography, scanning electron microscopy (REM), X-ray diffraction (XRD) and X-ray fluorescence (XRF) analysis. Furthermore, depth profile analyses were carried out on oxide and corrosion scales using glow discharge optical spectroscopy (GDOS), secondary neutral and ion mass-spectrometry (SNMS; SIMS), electron probe microanalysis (EPMA), and Rutherford backscattering spectroscopy (RBS). In the following sections, some examples will be discussed in detail.

Table 1 *Coating properties and methods of characterization (Underlined methods = non-destructuve testing)*[5]

passivation coating	surface topography	REM
	phase constancy	RFS, ESCA SIMS, (Raman)
	thickness	REM, EAS, SIMS, (ESCA), (LM)
	morphology	REM
	interface	deep etching + LM or REM
protective coating	phase constancy	ESSMA, RFS, SIMS, (Raman)
	Phase distribution	microreflection, pol. light, quant, image analysis
	conc. profiles/element distribution	ESMA, AES
	layer thickness	US, eddy current, β-backscattering (REM, LM)
	ductility	SEA
	structure	deep etching + LM or REM
	coating flaws (pores, cracks, inclusions etc.)	US, REM, LM
	transition zone	ESMA, AES, LM, REM, quant. image analysis
substrate		

3. GAS-COOLED HIGH TEMPERATURE REACTOR

The long-term use of coal as a source of energy will necessitate its conversion into liquid and gaseous hydrocarbons, e.g. in order to replace mineral oil. The processes currently available for coal liquefaction and gasification require two energy units of carbon to produce one energy unit of methanol. This can be significantly improved with respect to coal consumption and thus the CO_2 emission by advanced technologies, such as a symbiosis with nuclear energy or solar energy.

This implies the use of energy in the form of hydrogen which would be produced by nuclear or solar energy. The technology required for this purpose is not yet commercially operational, but its development is promising. A particularly important contribution towards such a symbiosis between coal and nuclear energy can be provided by the helium-cooled high-temperature reactor (HTR). The examples in Figure 1 show that the high temperature process heat reactor offers the prospect of nuclear heat production at a high temperature level suitable for a variety of chemical processes.

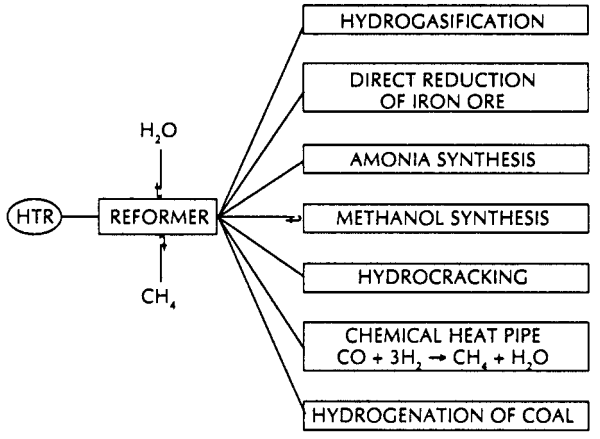

Fig. 1
Use of the high-temperature process heat reactor with pebble-bed core for various chemical processes

In Germany the HTR development is based on experience of more than 25 years. In Japan the construction of a small test reactor is on the way. Research activities are going on in USA, GUS, and the Peoples Republic of China. The German HTR reactor systems are characterized by the use of spherical graphitic fuel elements (600 mm in diameter), which for fission product retention, contain the fissile material in the form of coated particles[7,8]. These fuel elements as well as the used structural graphite have been sufficiently qualified, even for a long-term use under process heat reactor conditions. This means that for this area no new analytical methods are required.

3.1 Heat exchanging components under HTR conditions

Whereas it has been proved that the core components comply with their specification during the lifetime of a plant for both duel-cycle plants and HTR process heat systems, important investigations are still under way for verifying the design data for the heat extracting, highly stressed, metallic components, such as the steam reformer and the intermediate He/He heat exchanger tubes. For the construction of the heat exchanger components, Ni- and Fe-base alloys such as $NiCr_{23}Co_{12}Mo$ (Alloy 617) and X10NiCrAlTi32 20 (Alloy 800) are used. These components are operated at temperatures between 550 and 1000 °C in which range the structural alloys exhibit clearly time-dependent properties (creep and fatigue behaviour). The integrity of these components is assured by the exclusion of spontaneous large-area failures. The database required has been established during the past decade in a broadly based materials testing programme for steam reformers and intermediate He/He heat exchangers with design lifetimess of more than 100 000 hours. From the wide range of methods used for characterization, the tasks and problems involved in corrosion studies on metallic materials for the HTR primary circuit will be dealt with.

3.1.1 Properties after long-time annealing

After long-time use at high temperatures, high temperature alloys generally undergo structural changes resulting in a decrease in deformability at room temperature. Precise statements on the short-time characteristics at the end-of-life can be derived by testing specimens after a simulated service 600 and 950°C, for example, leads to the precipitation of new phases and to the transformation of existing phases in the microstructure of the high temperature alloys used. The analytical determination of the precipitated phases is of particular significance owing to the influence of these structural changes on the mechanical properties. For this purpose, the following method is used.

Time-temperature-precipitation diagrams after long-time exposure were prepared after chemical isolation and identification of the structural constituents (Figure 2). For the qualitative and quantitative determination of the individual phases XRD, XRF and TEM were used in addition to optical microscopy image analysis, EPMA and REM. Owing to the complexity of precipitates in high temperature alloys, standards must first be prepared for quantification.

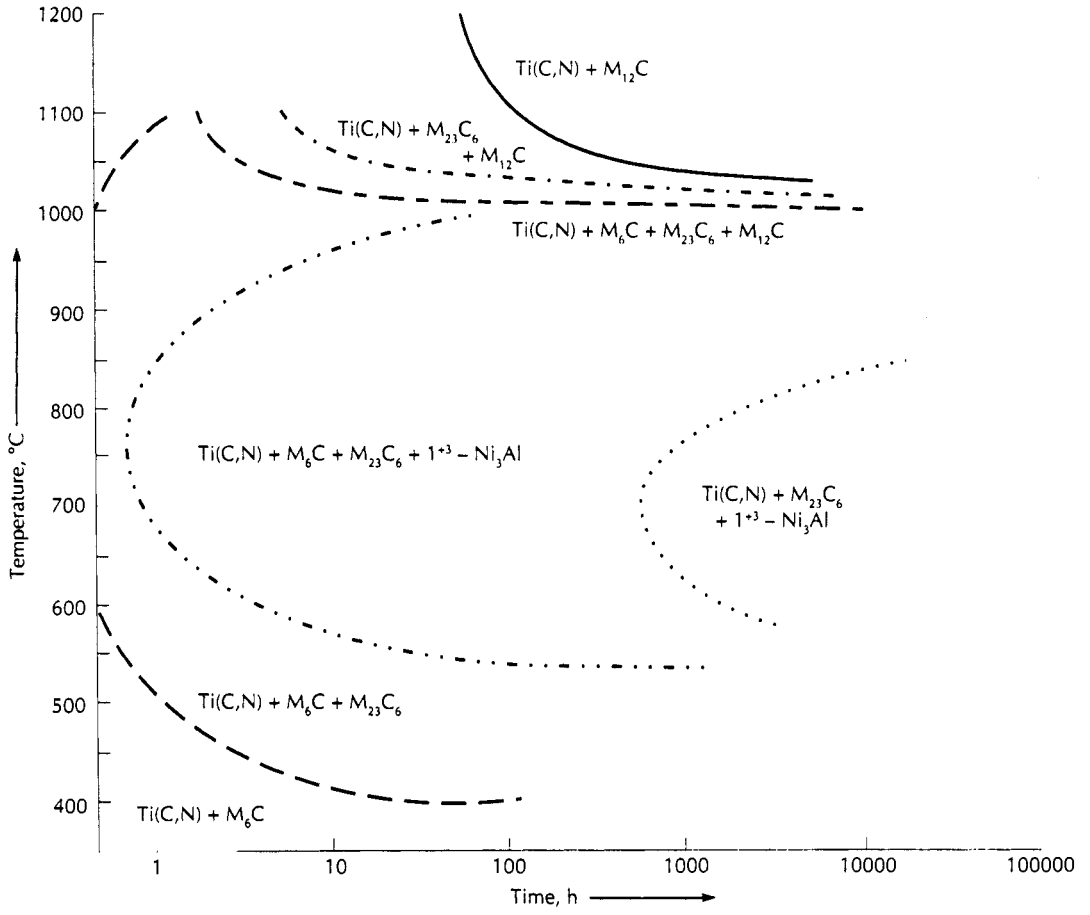

Fig. 2. Time-temperature-precipitation diagram for INCONEL 617 alloy

3.1.2 Corrosion in HTR helium

The mechanical properties at room temperature and at the operating temperatures can be modified by internal oxidation and/or carburization which can occur due to the effect of impurities such as H_2, H_2O, CO, CH_4, CO_2 in the μ-bar-range in the primary circuit helium gas. The discussion will only refer to the corrosion system HTR helium and high temperature alloys. Methane and carbon monoxide can have a carburizing effect due to the low oxygen partial pressure. A carburization process especially with chromium and molybdenum in the alloys used here would lead to the formation of carbides which reduce the ductility in the range between room temperature and approximately 700°C. This must be taken into consideration in the design and operation of the heat exchanging components. The loss in ductility can be avoided if a dense oxide layer is formed on the alloys which acts as a barrier against penetrating carbon.

Analytical surface chemistry is of particular significance for the deposition of carbon from the gas phase, characterization of the surface scale on the alloy, the permeation of carbon through the surface scale, the characterization of the surface of the metallic matrix and the uptake of carbon into the metal.

A resolution of <0,1 μm in the horizontal and vertical direction is desirable for analysing the phases and showing the microstructure. The low electrical conductivity of the oxides for the signal generating electron or ion beam represents a special problem. In order to avoid excessive carbon uptake or to obtain a significant reduction of hydrogen and tritium permeation, attempts are being made to produce dense,

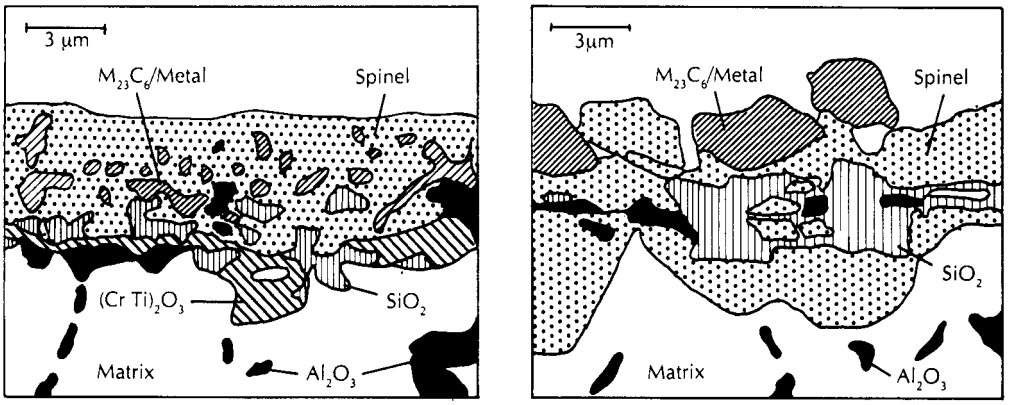

10 000 h, 800°C 10 000 h, 900°C

Fig. 3. Effect of temperature on scale formation; Alloy 800 H exposed in HTGR helium

influencing the gas impurity composition or adequately designing the gas purification system may also be used to alleviate corrosion effects. The oxides scales consist of Cr, Ti, Al or Si oxides with mixed oxides (spinels). The large variety of experimental findings in a simulated HTR helium atmosphere led to a systematic investigation of the influence of different contents and partial pressure ratios of gas contamination on material corrosion. Figure 3 shows two typical examples of surface scales formed in HTR helium.

The application of EPMA combined with XRD leads to the semi-quantitative determination of both oxide and carbide corrosion products. As an example Figure 4 shows the X-ray diffraction diagram of the surface of an exposed Alloy 800H specimen. The following four crystalline phases were identified: the two carbides $M_{23}C_6$ (cubic) and M_7C_3 (hexagonal) as well as the two oxides M_3O_4 (spinel type) and M2O3 (corundum type)9.

3.2 Characterization of oxide scales on high temperature alloys

The Ni- and Fe-based alloys contain about 20% Cr as well as small amounts of elements such as manganese, aluminium, titanium, silicon and sometimes yttrium. These elements have a high affinity for oxygen and are therefore also oxidized in an atmosphere with low oxygen partial pressure. For understanding the oxidation and/or the corrosion mechanisms it is necessary to determine the depth profiles quantitatively if possible, by using the above-mentioned methods in combined forms. In the following sections, some examples will be described.

3.2.1 Integrating methods for the analysis of oxide scales using GDOS, EPMA and SNMS

The investigations were carried out on an oxidized high-temperature alloy, Alloy 617. Oxidation took place in air at 900°C for 1000 h. In addition to the classical metallurgical investigation techniques, such as metallography and X-ray diffraction analysis for the verification and calibration of the depth profiles measured by GDOS, other surfaces analysis methods (EPMA and SNMS) have been used[10]. In the case of the GDOS analysis reference compacts from powder mixtures of Cr, Mn and Ti and of the corresponding oxides with Cu as bonding material were investigated.

In order to ensure comparability of profile measurements by electron microprobe analysis with a procedure that already allows integration opver a larger surface area (burning spot) owing to its excitation conditions, local averaging must be analogously combined with the measuring process. Since microprobe measurements use a metallographic cross-section of the oxidized specimen, the measuring surface to be integrated can only be scanned on-dimensionally instead of two-dimensionally.

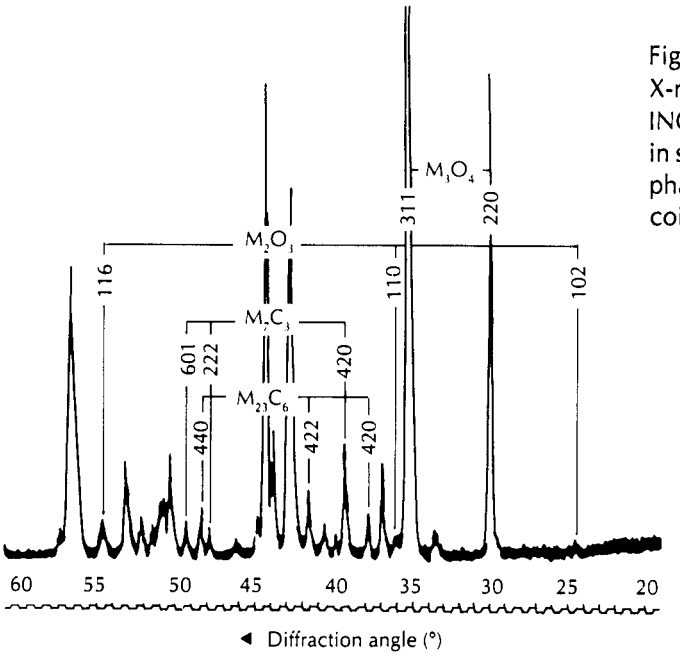

Fig. 4
X-ray diffraction diagram of the surface of INCOLOY 800 H after 10 000 h at 850°C in simulated reactor helium. For each phase the most intense peaks without coincidence are marked[9]

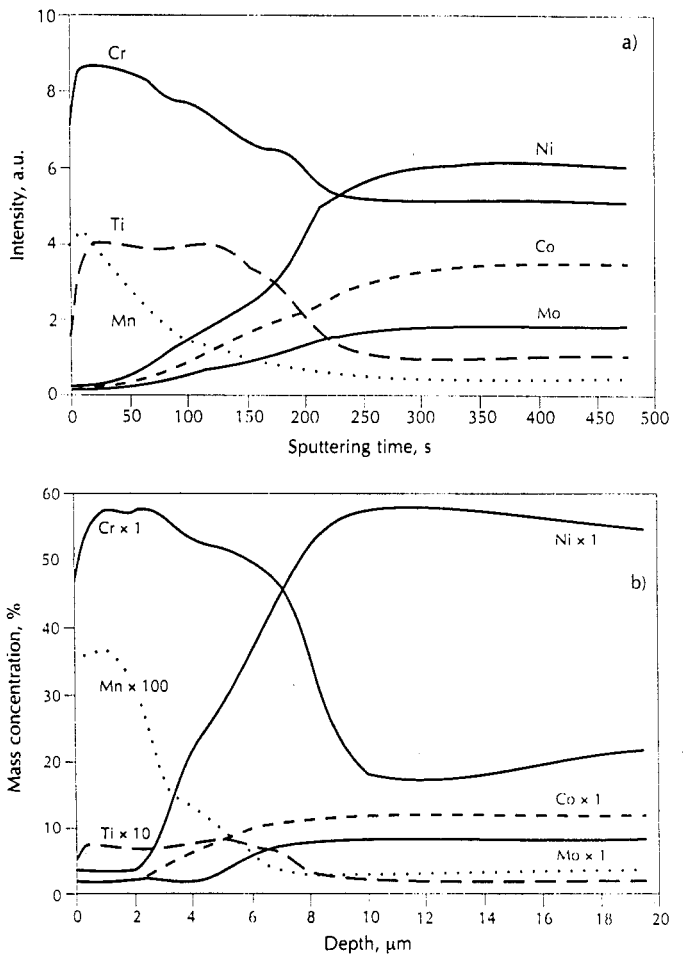

Fig. 5. GDOS (a) intensity time curves; (b) concentration depth profiles for Cr, Mn, Ti, Ni, Co and Mo in oxidized INCONEL 617 alloy

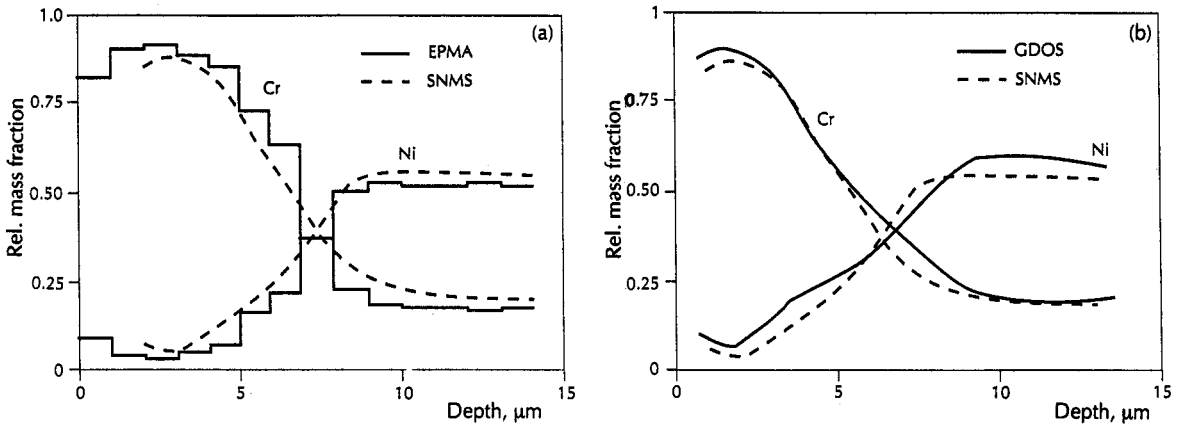

Fig. 6. Oxidized INCONEL 617 alloy, comparison of (a) EPMA and SNMS; (b) GDOS and SNMS depth profiles

According to this principle, the conventional point analysis in profile measurements by step scanning technique is modified in that the focussed electron beam is linearly oscillated by fast electromagnetic deflection transverse to the profile direction.

The area covered by the electron beam must be selected so as to provide reproducible local average values which are representative of the chemical composition at this layer depth. Under these conditions it may be expected that the profiles thus obtained are comparable with the results of other methods involving automatic integration.

In order to justify the above described procedure of introducing mass fractions and to confirm the analytical results obtained by the GDOS and EPMA methods, quantitative depth profiles were recorded by the SNMS direct bombardment mode on specimens examined[11]. The analysis of the oxidized high-temperature alloys was carried out by Leybold AG using the INA-3 device.

For a combined representation of the results, quantitative comparison requires fitting for both the position coordinates of the layer thickness and the element concentration. For this purpose, the quantified element profiles for the GDOS analysis and SNMS reference measurements were converted into relative mass fractions and representated together with the EPMA results, e.g. for the two elements Ni–Cr on a uniform scale in Figure 6a, b. The profiless of these elements are generally characterized by good agreement in the local pattern and in most cases also in the quantitative proportions. Deviations between the individual methods may be regarded as negligible.

A surprising result is the increase in the Ni/Cr ratio from inner to outer layer region for all methods. This observation may be explained by a spinel formation in agreement with the results of X-ray diffraction. The lattice parameter of a = 836 pm measured for the spinel phase is indeed indicative of the $(Ni,Co)Cr_2O_4$ composition, and mixed with small amounts of Mn_2TiO_3.

3.2.2 Quantifying the GDOS depth profiles

The GD simultaneous spectrometer SPECTRUMAT S 1000 used permits three different modes of operation for glow discharge control: (a) stable voltage (U = constant); (b) stable current (i = constant); and (c) stable power (P = U·i = constant). Each of these operating modes provides different intensity-time profiles for the same oxide scale system. It should be noted that the sputtering times for different scales and the line intensities are very different despite nearly the same glow discharge power. A simple transfer of the intensity conditions to the concentrations generally leads to wrong conclusions. This is due to different sputtering rates in the oxides and the alloy and to different effects of voltage and current changes on sputtering. In Figure 7 it is shown that the U-i curve of glow discharge with INCONEL alloy 617 as the target is steeper than with oxide. This means that the charge carrier density in the plasma is lower for the alloy than for oxide.

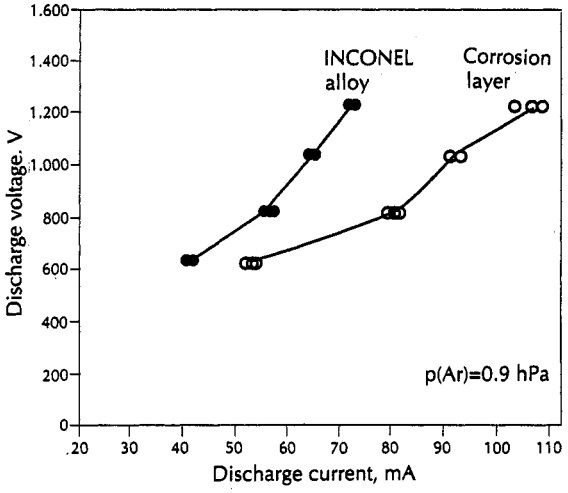

Fig. 7. U-i curve of glow discharge for INCONEL alloy 617 and oxide scale

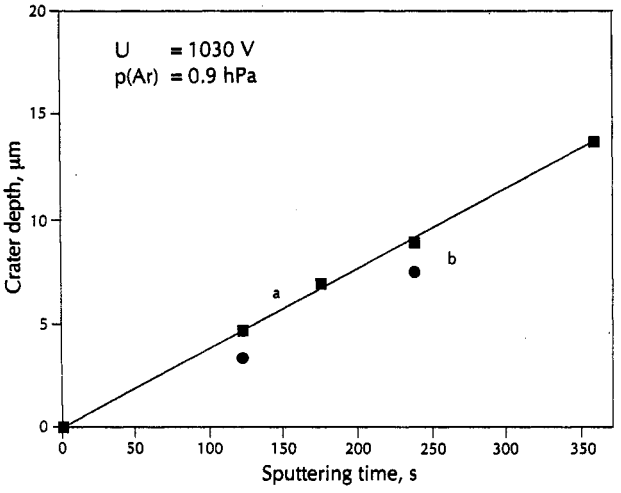

Fig. 8. Crater depth in the oxide scale as a function of sputtering time: (a) obtained by crater profile measurement; (b) calculated from weight loss

The intensity-time curve at U = constant reflects best the concentration profile of the individual elements perpendicular to the surface. At constant Ar pressure (p(Ar=0,9 h Pa) and discharge at stable voltage (U = 1030 V), the mean free path of the primary charge carriers remains approximately constant in the plasma volume. The Ar ions thus hit the target with constant average kinetic energy irrespective of whether the oxide scale or matrix material is sputtered. The change in discharge current intensity from layer to layer into the matrix material is indicative of differences in charge carrier generation at different depths. This generation involves a superposition of sputtering effects, secondary electron production and ionization processes of the sputtered target material in the plasma.

In Figure 5a the GDOS intensity time curves and in Figure 5b the concentration depth profiles for the elements Cr, Mn, Ti, Ni, Co and Mo in oxidized INCONEL 617 alloy are shown. Conversion of the time axis into depth values was effected by calibrating the time-dependent depth on the basis of the measured crater depth (Figure 8).

Because of the lack of calibration specimen series for oxide scale analysis, the transformation of qualitative intensity-time profiles into quantitative concentration-depth profiles require the experimental determination of empirical correlations between glow discharge parameters (voltage, current intensity), sputter rate, and element concentration with line intensity. The intensity $I_{\lambda,E}$ of the spectral line λ of the element E is calculated as follows according to [12]:

$$I_{\lambda,E(S)} = R_{\lambda,E(S)}\,(i,U)\cdot C_{E(S)}\cdot V_S(i,U) \quad \ldots\ldots(1)$$

where $R_{\lambda,E(S)}$ is the emission factor for the spectral line of the element E in the sample. $C_{E(S)}$ is the mass concentration of the element E in the sample and V_S is the sputter rate of the sample (mass loss per unit of time).

The change of the emission factor $R_{\lambda,E}$ due to the current intensity is taken into account by equation (2) with $r_{\lambda,E}$ as the specific emission factor:

$$R_{\lambda,E(S)}\,(i,U) = r_{\lambda,E(S)}\,(U)\cdot i_s \quad \ldots\ldots(2)$$

Substituting equation (2) into equation (1) lead to

$$I_{\lambda,E(S)} = r_{\lambda,E(S)}(U)\cdot i_S\cdot C_{E(S)}\cdot V_S(i_S,U) \quad \ldots\ldots(3)$$

The corresponding equation for the reference sample reads:

$$I_{\lambda,E(Ref)} = r_{\lambda,E(Ref)}(U) \cdot i_{Ref} \cdot C_{E(Ref)} \cdot V_{Ref}(i_{Ref}, U) \quad \ldots\ldots(4)$$

The ratio (3)/(4) is formed for $C_{E(S)}$ as:

$$C_{E(S)} = C_{E(Ref)} \frac{I_{\lambda,E(S)} r_{\lambda,E(Ref)}(U) V_{Ref}(i_{Ref}, U) i_{Ref}}{I_{\lambda,E(Ref)} r_{\lambda,E(S)}(U) V_S(i_s, U) i_s} \quad \ldots\ldots(5)$$

The investigations of matrix effects revealed that the specific emission factor is independent of the matrix within the error limits for all the elements examined and also independent of the chemical bonding state for the elements Cr, Ti, and Mn so that the correction factor for specific emission in equation (5) becomes 1. This reduces the calculation of the concentration according to equation (5) to corrections with respect to the sputter rates and discharge currents.

4. CHEMICAL ENGINEERING AND ENERGY CONVERSION

Increased efficiency of processes in chemical engineering and energy conversion can in many cases only be achieved if the process temperatures are increased. This requirement necessarily leads to the demand for metallic materials which allow the design of plant or engine components operating at high temperature often at high stresses in corrosive environments. Oxide dispersion strengthened (ODS) alloys are potentially suitable construction materials for components which are subjected to hostile service conditions due to their unique combination of superior high temperature creep and corrosion resistance[13]. Especially in cases where component life is limited by corrosive attack, ODS alloys offer the possibility for significantly increased service lives due to improved component integrity.

4.1 Oxide dispersion strengthened (ODS) alloys

High temperature nickel-, cobalt- and iron-based alloys are strengthened by a combination of solid solution and precipitation hardening. The effectiveness of both strengthening mechanisms strongly decreases at higher temperatures, and consequently these alloys are not suitable construction materials for highly stressed components which have to operate for very long times at temperatures significantly above around 950°C. ODS alloys contain small amounts (~0,5-1 mass.%) of a finely dispersed oxide phase (mostly yttria) which is thermodynamically much more stable than the strengthening particles, such as 'gamma prime' (γ') and carbides, present in conventional high temperature alloys. Therefore the strengthening imparted by the oxide dispersions is retained up to very high temperatures because coarsening or dissolution of the particles does not occur. In addition, the presence of the dispersions allows a very coarse alloy microstructure to stabilize over long exposure times. This leads to excellent creep resistance up to much higher temperatures than can be achieved with conventioned wrought or cast alloys. ODS alloys are produced by high energy milling powder mixtures of the alloying elements and/or master alloys with the oxide dispersion. The mechanically alloyed (MA) powder is compacted by extrusion. With suitable heat treatments the desired coarse, elongated grain structure can be achieved. Examples of commercial iron- and nickel-based ODS alloys are given in Table 2. Figure 9

Table 2 *Nominal composition of commercially available iron- and nickel-based ODS-alloys. All ODS materials used in the present study were supplied by H. Wiggin, Hereford, UK*

Alloys	Composition in Mass.-%									
	Ni	Fe	Cr	Al	Ti	W	Mo	Ta	C	Y_2O_3
MA 956	–	Base	20	4,5	0,3	–	–	–	0,04	0,5
MA 754	Base	–	20	0,2	0,3	–	–	–	0,04	0,5
MA 6000	Base	–	15	4,5	2	2	2	2	0,04	1
MA 760	Base	–	20	6	–	3,5	2	–	0,04	1

compares the creep resistance of two ODS alloys with that of the conventional γ'-strengthened cast turbine material IN 738. At lower temperatures the nickel–chromium ODS alloy MA 754 is weaker than the γ' hardened material. At higher temperatures, however, MA 754 is superior in spite of its simple composition. MA 6000, which is strengthened by dispersion- as well as γ'-hardening, is stronger than IN 738 in the whole temperature range.

4.1.1 Growth, adherence and composition of oxide scales

For their high temperature oxidation/corrosion resistance the nickel- and iron-based ODS alloys rely on the formation of slowly growing and well adherence chromia and alumina scales. In the next sections the oxidation properties of MA 754 will be chosen as an example for chromia forming alloys, MA 956 for any alumina forming materials. The results will be compared with those obtained for conventionally produced wrought alloys Ni-25Cr and Fe-20Cr-5Al.

Figure 10 shows mass changes as a function of time for alloyt MA 754 and the conventionally produced alloy Ni-25Cr during cyclic oxidation at 1000°C. The ODS alloy shows lower oxide growth rates and better spalling resistance than Ni-25Cr. Figure 11 compares X-ray diffraction analysis of the surface scales after 300 h isothermal oxidation at 1000°C. The ODS alloy clearly exhibits a very selective oxidation of chromium whereas the scale on Ni-25Cr contained significant amounts of $NiCr_2O_4$ and NiO in addition to chromia. Isothermal and cyclic oxidation of the alumina former MA 956 and the conventionally produced wrought alloy Fe-20Cr-5Al shows that the differences in oxidation behaviour between ODS- and non-ODS alloy are similar to those observed for the chromia formers: the spalling resistance of the scale on the ODS alloy is far better and the scale growth is slower than that on Fe-20Cr-5Al.

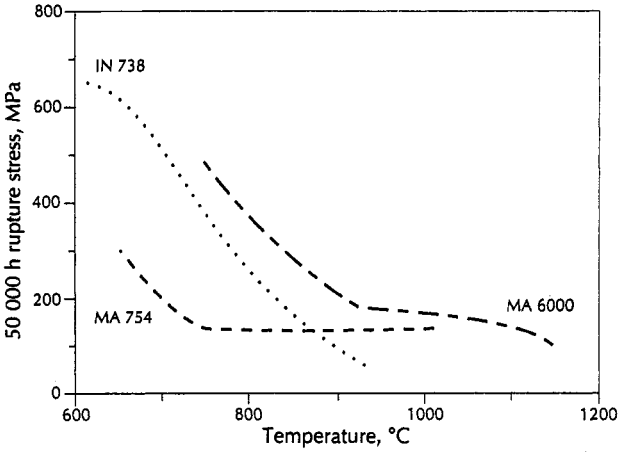

Fig. 9. Temperature dependence of creep strength for MA 6000 and MA 754 compared with that of the g'-strengthened cast alloy IN 738

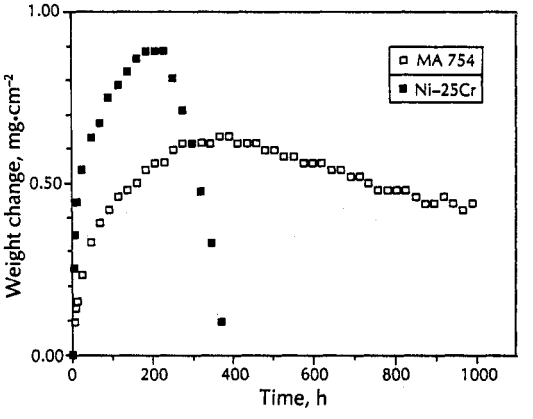

Fig. 10. Cyclic oxidation of MA 754 and Ni-25Cr at 1000°C in synthetic air. Each cycle consisted of 56 minutes heating and 4 minutes cooling[13]

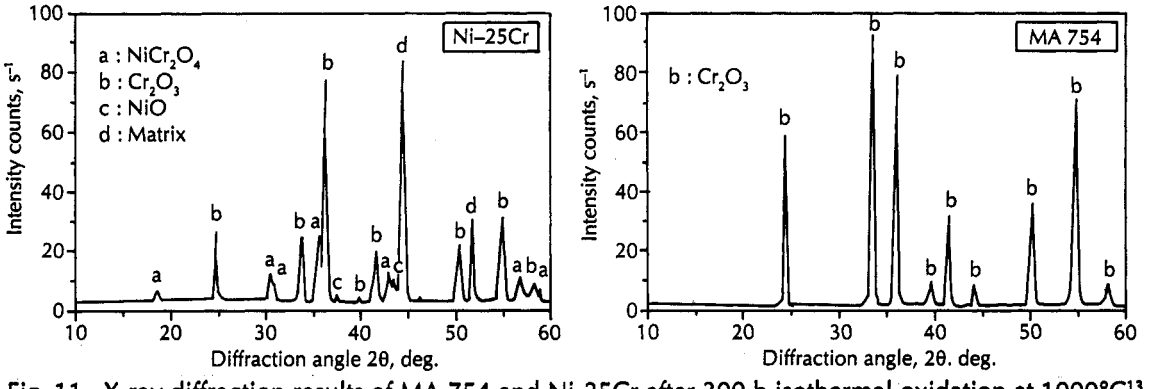

Fig. 11. X-ray diffraction results of MA 754 and Ni-25Cr after 300 h isothermal oxidation at 1000°C[13]

4.1.2 Investigation of the growth mechanisms of protective chromia and alumina scales

As an example the positive influence of a Y_2O_3 dispersion on the oxidation resistance is correlated with a change in the growth mechanisms of the scale[14,15]. For this purpose, the oxidation behaviour of two ODS alloys, MA 954 (the chromium oxide former Ni-20Cr-0,5Y_2O_3) and MA 956 (the aluminium oxide former Fe-20Cr-5Al-0,5Y_2O_3) was compared with that of two conventional wrought alloys, Ni-25Cr and Fe-20Cr-5Al. The growth mechanisms of the scales were examined by a two-stage oxidation method with ^{18}O as tracer, the distribution of the oxygen isotopes in the oxide scale being determined by SIMS.

The results have shown that both ODS alloys exhibit a more selective oxidation of the scale-forming alloying elements than the conventional alloys.

Figure 12 shows depth profiles (measured by SIMS) for the oxygen isotopes ^{18}O and ^{16}O in the oxide layer on the aluminium oxide formers after different oxidation steps in air at 1000°C. The results show that the scales on Fe-20Cr-5Al grow by cation transport to the scales-gas interface as well as by oxygen transport to the scale-alloy interface: the ^{16}O introduced in the second oxidation stage is clearly seen to be enriched near the interface. This is also the case for the ODS alloys, however, the enrichment at the scale-gas interface, especially for the shown MA 956, is essentially smaller than for the conventional alloy. This shows that for the ODS alloys the cation transport is reduced and mades only a small contribution to the overall oxide growth; the layer grows almost exclusively by oxygen transport.

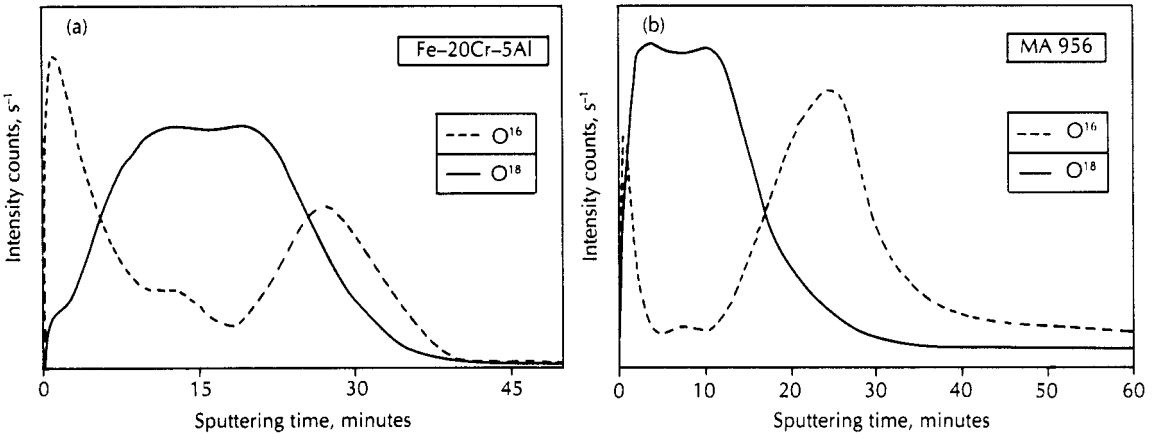

Fig. 12. Distribution of the oxygen isotopes ^{18}O and ^{16}O in the oxide layer on the aluminium oxide formers after 3 h of oxidation in ^{18}O-enriched air followed by 9 h of oxidation in normal air at 1000°C[14,15]

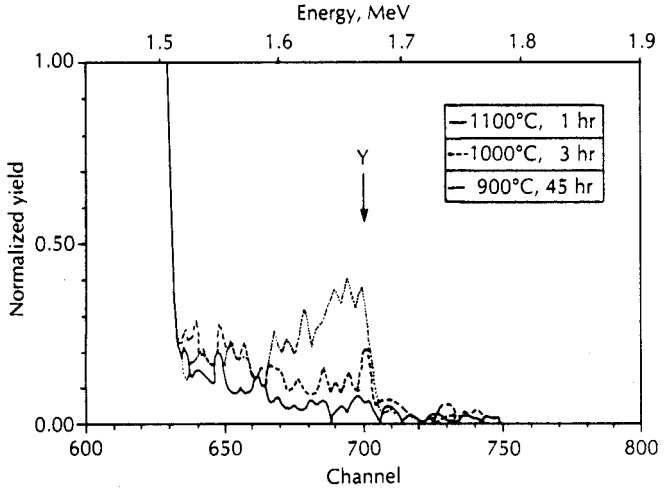

Fig. 13
RBS analysis of oxide scales on alloy MA 956 after different oxidation times in the temperature range 900–1100°C[14,15]

The oxidation experiments with the aluminia- and chromia-forming ODS alloys have demonstrated that additions of yttria decrease the oxide growth rate, improve scale adherence, and enhance selective oxidation. The addition of Y_2O_3 significantly reduces the outward growth by reducing the outward cation transport. Decreased cation transport reduces pore formation at the scale-metal interface, as a result of vacancy condensation and thereby prevents the formation of a convoluted, poorly adherent scale. Decreased transport of nickel and/or iron cations reduces spinel oxide formation and consequently enhances selective oxidation. Detailed analysis of oxide scales by scanning transmission electron microscopy has shown that yttrium tends to be enriched at the grain boundaries in Al_2O_3 and Cr_2O_3 scales[16]. For analysing the oxide on the ODS alloy MA 956 after different oxidation times in the temperature range 900–1000°C the Rutherford backscattering method has also been used. The results in Figure 13 confirm that yttrium is concentrated at the outer surface of the oxide films.

5. STRUCTURAL CERAMICS

Oxide and carbide ceramic materials, graphite and other carbon based materials are used for structural components in high temperature applications. For determining the structure, the stability and the phase diagrams as well as the physical, chemical and mechanical properties of the ceramic materials the quantitative concentration of the main elements as well as the impurities is a crucial requirement. In the following section some examples will be explained.

5.1 Silicon carbide

Due to their high temperature strength, high temperature stability, good thermal conductivity and corrosion resistance, silicon carbide ceramics as SSiC or SiSiC are used in various technical applications e.g. heat exchanging components, chemical reaction tubes, combustion systems, sliding rings, solar receiver for operation temperatures above 1000°C17 and high heat flux fusion components (see Chapter 6).

5.1.1 High temperature corrosion of silicon carbide materials by different gaseous environments

For the above-mentioned applications it is necessary to know the influence of corrosion by various gases and gas mixtures at high temperatures on the strength of these materials. Silicon carbide is known to resist oxidizing atmospheres by forming a protective silicon dioxide layer. In reducing atmospheres, however, active corrosion may occur with formation of volatile silicon compounds, e.g. SiO, $SiCl_4$, $SiCl_2$ and SiC. Some aspects of silicon carbide corrosion will be described after exposure to atmospheres containing water vapour, hydrogen, nitrogen, and, in some cases, sulphur dioxide, hydrogen sulphide, and hydrogen chloride at temperatures between 1100 and 1400°C[18].

After exposure to hot water vapour/hydrogen atmospheres, the silicon carbide specimens were found to be covered with layers of silicon dioxide which were identified by X-ray diffraction to be mainly α-cristobalite. Scanning electron microscopy of fracture surfaces showed thin and dense oxide layers on SiSiC (Si-rich SiC) and on sintered SiC containing about 0,3% Al as a sintering aid (SSiC(Al)). The corrosion rate of SiSiC and SSiC(Al) is controlled by the oxygen diffusion in the dense oxide layers on the surface of the specimens.

Corrosion tests on SiSiC (with 18% free silicon) at 1240°C for 720 h in a water vapour/hydrogen/nitrogen atmosphere show an increase in the mean bending strength (from 322 to 421 MPa). By means of EPMA investigations of exposed SiSiC samples, nitride inclusions were detected (together with oxide) within a reaction zone of about 30–50 μm below the silicon oxide layer.

No corrosive attack of the SiSiC could be observed after 168 h at 1105°C in air with 1% HCl. Contrary to this result, severe corrosive attack was observed if SiSiC was exposed to 1% HCl under the same conditions, but in a reducing atmosphere of dry H_2/N_2 mixture (the mean bending strength was reduced from 322 to 99 MPa). The extent of volatized Si phase depends strongly on temperature. No silicon loss

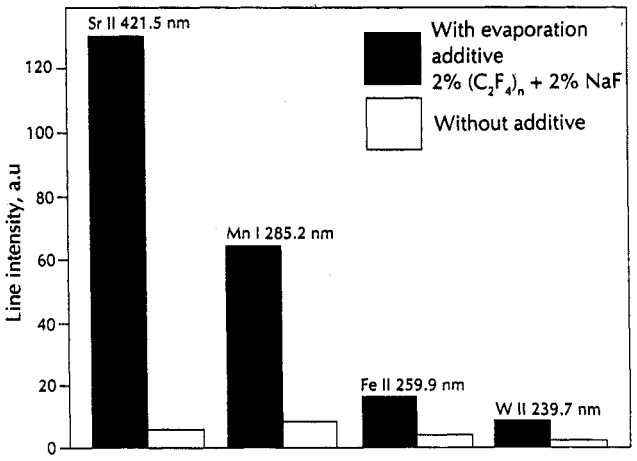

Fig. 14. Line intensities for Sr, Mg, Fe and W with and without additives (DSID)

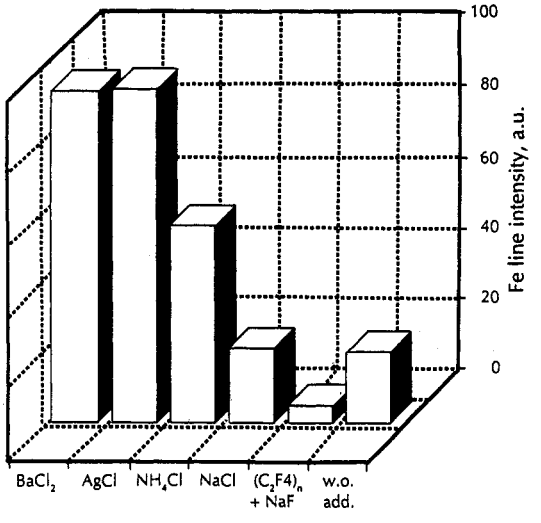

Fig. 15. Influence of different thermochemical additives on the line intensity of Fe in Durital E 90 at 2000°C furnace temperature

occurred below 1090°C, at 1105°C about 50% (Figure 15) and above 1110°C 100% of the Si phase disappeared. The resulting open porosity is the reason for the decreased bending strength.

In summary, the very different corrosion conditions depend on stoichiometry, structure, sintering aids, distribution of free silicon phase and temperature.

5.2 Direct determination of impurities in ceramics by inductively coupled plasma-atomic emission spectrometry (ICP-IES) using direct sample insertion (DSI) or external electrothermal vaporisation (ETV)

The development of direct methods for the determination and routine control of impurities in powdered ceramic material is required. The analysis of refractory powders is possible by either direct introduction into ICP, slurry technique or transport into ICP of a dry aerosol, externally formed by electrothermal vaporisation.

In earlier studies with the inductively coupled plasma optical emission spectrometry (ICP-OES) it could be shown that beside the direct sample insertion device of powder material (DSI) the external electrothermal evaporation analysis (ETV) is a promising method in the analysis of ceramic powders for elements which are volatile or form volatile compounds as a result of thermochemical reactions[19,20]. Knowledge of powder composition and behaviour in the electrode as well as of the formed volatile compounds is of decisive significance since even small amounts of trace impurities can lead to indesirable chemical-physical effects or to ceramic component failure due to accelerated crack growth. It is also possible to influence positively the behaviour of structural ceramic materials by selectively adding various substances in lowest concentrations. Rapid and accurate control is therefore required during production of this type of ceramic materials.

From the literature cited in Ref. 19,20 the advantages of ICP (high accuracy and low detection limits) can be increased by coupling to an external vaporization unit. Sample preparation time is shortened since the specimen need to be dissolved. Avoiding dilution increases the detection capability, since sources of error due to additional contamination of sample material can be ruled out.

5.2.1 Determination of impurities in graphite and alumina-based ceramics

It is known that the combination between DSI and ETV with ICP-AES produces a promising method for analysis of ceramic powders especially for volatile elements or elements which form volatile compounds as a result of thermochemical reactions. Successful chemical modification is becoming a key operational factor. In the case of the graphitic powder sample a positive influence on the vaporization processes could be achieved by using $(C_2F_4)_n$ and NaF as thermochemical additive. Nearly 100% of the sample quantity used was found to be vaporized within a few seconds. In the absence of an additive, this could not be realized, not even after 5 min. Moreover, use of the additives resulted in a considerable increase in the measured line intensity for impurities in graphite (Figure 14). A similar result by using different additives or so called modifiers has been achieved in the analysis of the alumina-based ceramic powder Durital E 90 with ETV-technique. Figure 15 compares the influences of different additives on the intensity of an iron line at a constant temperature of 2000°C in the heating device. The optimum ratio of line intensity to underground I/I_0 is obtained using the metal chloride AgCl and $BaCl_2$. Sodium in NaCl reduces the excitation processes of iron in the plasma. Based on radioactive ^{59}Fe data, no effect of using the carrier mixture $(C_2F_4)_n$+NaF on the vaporization of iron could be detected. The presence of sodium leads to a decrease in the Fe line intensity below that of original substance without additives.

The efficiency of the apparatus was tested for a powdered graphite and ceramic matrix under the experimental conditions for sample vaporization listed in Table 3. The experiments show as a special feature of ETV the fact that both the heating time and the heating temperature can be chosen, whereas in DSI only the heating time can be freely selected. The volatilization of Fe, in particular, has been shown to depend strongly on the use of an additive in both cases. This is readily shown by the tracer studies applied. The studies of Cd at the same time clearly showed that the carriers selected led to a decrease of the excitation efficiency and thus were useless in the case of a very volatile element. In DSI, Fe could be almost completely volatilized from a graphite matrix with 10s when a suitable additive was used, whereas in the ceramic its volatilization efficiency was better then 90%.

Table 3 *Comparison of DSI and ETV*

	DSI	ETV
T_{max}	3000°C	3000°C (variable)
T depends on	position of crucible	power variation up to 3 kW
$\partial T/\partial t$ depends on	speed of crucible in the plasma	Voltage variation (25–800°C/s)
t	variable	0–5 s
Evaporation	100%	~ 80%
Line intensity I_x/I_{DSID}	1	~ 0,8
RSD (line intensity)	± 10%	± 8%
Detection limit for Fe	~ 10 ng/g	~ 10 ng/g

5.2.2 Optimization of ETV-ICP-IES method for the determination of impurity elements in SiC powder

The aim of the investigation was to clarify the principal importance of the thermochemical processes in ETV-ICP-IES analysis by using chemical modifiers on the vaporization and quantitative determination of impurities in SiC powders[21]. to fulfil the requirement of the quantitative analysis the following two procedures have been combined: a) separation of sample evaporation from atomisation and excitation and b) the 'in situ processing' in the sample container. It is well known that it will be impossible to achieve total vaporization of the most carbide forming elements from ceramic or refractory powders without chemical reactions. In the literature the necessity of using modifiers to improve the vaporization of carbide forming elements in such materials has been demonstrated on the basis of our own experiences for the quantitative determination of impurities in SiC-powder, a combination of BaO+CoF2 (1:1) has been used as an optimal modifier. This complex modifier destroys almost totally the SiC thus enabling the evaporation of the impurities. The products identified after the thermochemical reaction in the rest in the electrothermally heated graphite crucible are: Ba_2SiO_3, $CoSi(CoSi_2)$ and BaF_2 (Figure 18).

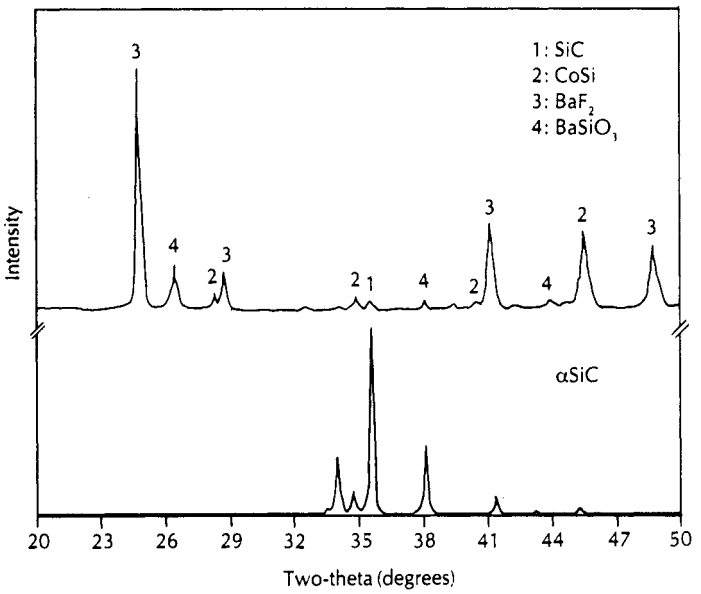

Fig. 16. X-ray diffraction patterns of SiC without treatment and of the material remaining in the crucible after the action of the thermochemical modifier $BaO:CoF_2$ = 1:1. The comparison demonstrate a total destruction of SiC

For the general feature of reactions at high temperatures the complex reaction processes are discussed by thermodynamic calculations. The results of the temperature dependence of the isothermal isobaric potential for the reaction of SiC with the used modifier BaO + CoF_2 are shown in Figure 17. Summarizing the results has shown that the data of the thermodynamic calculation and the experiments are in good agreement. Following this mode one can modify in principle every type of powdered sample to the desired extent and manner in an electrothermally heated graphite crucible.

6. FUSION REACTOR TECHNOLOGY

Fusion reactors for commercial energy production cannot be expected to be viable before the year 2030. Despite this fact, problems relating to the technical feasibility of fusion reactors have been investigated worldwide in recent years after successful research in the field of fusion-orientated plasma physics, especially concerning the magnetic confinement of plasmas. This also includes magnet technology, various materials problems, tritium and blanket technology, plasma-wall interaction and the problems of energy extraction. Work is focussed on research into the power balance and power density in fusion plasma, into thermal insulation and energy extraction to the outside and into power densities and material stressing in the plasma chamber blanket especially of a D-T Tokamak reactor system. At the KFA Jülich, the TEXTOR device (Torus Experiment for Technology Orientated Research) has been operated since 1982 in association with EURATOM, the main emphasis being on studies of plasma-wall interactions[22].

6.1 Plasma-wall interaction of highly stressed components

The first-wall is the wall of the combustion chamber surrounding the plasma. In stationary operation it absorbs with its components 20% of the fusion power emitted from the plasma in the form of radiation or particles fluxes. The materials for the highly stressed components of the first wall are subjected to plasma-wall interaction. The vacuum vessel or liner and other active first-wall components such as radiofrequency antennas for the ion cyclotron resonance heating, ICRH, are protected by limiters against direct plasma contact. In larger Tokamak facilities like NET (Next European Torus) or ITER (International Thermonuclear Experimental Reactor) divertors are used. This applies especially to

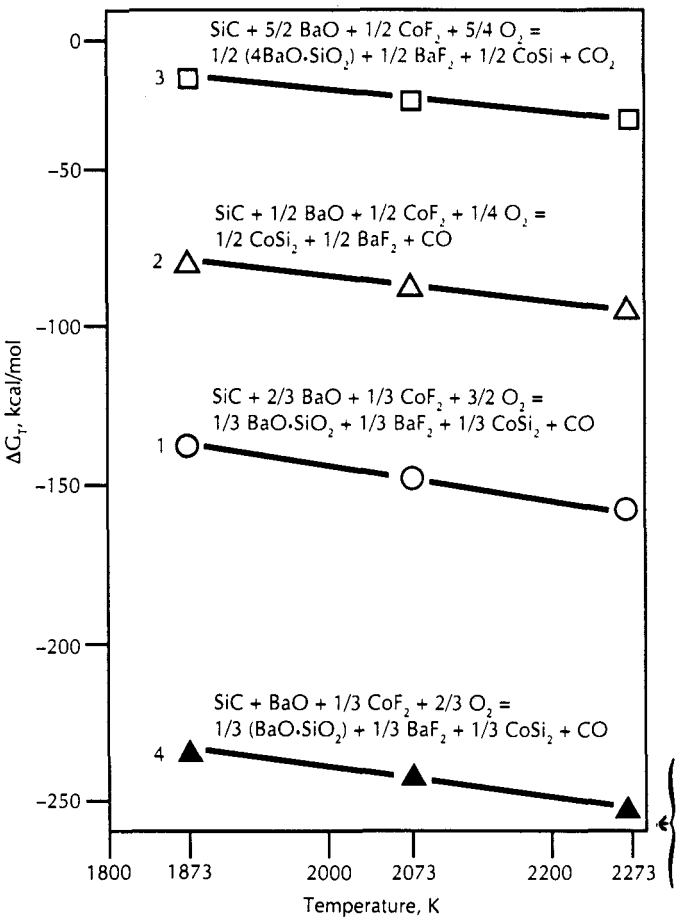

Fig. 17. The temperature dependence of the isothermal-isobaric potential for the following reactions between SiC and the complex modifier $BaO + CoF_2$

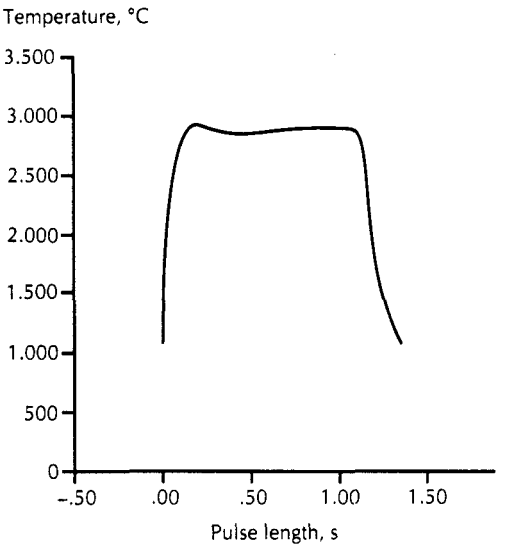

Fig. 18. Electron beam high heat flux tests on SiC Coat-Mix material

unstable plasma conditions or plasma conditions with low particle densities. These components exposed to high thermal loads are subjected to the same interaction processes as the vacuum vessel and liner during normal operation of a fusion reactor.

However, the effects on the limiter or divertor materials are considerably more intensive even in normal operation since these extend into the plasma boundary layer.

6.2 Plasma-induced damage and investigation of materials

Today all existing Tokamak machines operate with low Z material (low atomic number) walls. This is due to the fact that impurities with high Z materials contribute significantly to radiation losses from the hot plasma core. Therefore, a low Z number of the first-wall — at least for the plasma-facing side of the first-wall — has been realized in almost all thermonuclear confinement experiments today; in these machines, graphite or other carbon-based materials and cerammics are used as prime candidates.

The structural changes and damage induced by the hot plasma in the first-wall materials of tokamaks can be broken down into two groups of interaction: (a) normal operation; (b) unstable conditions.

During normal operation of a plasma machine, material is removed from the first-wall and its components by neutral particles and especially by ions and electrons. Unipolar arcs, i.e. microscopically small electric arcs, are formed between the plasma boundary layer and the surface of first-wall components. They can move across the material surface at right angles to the magnetic field lines causing local melting and evaporation of the material so as to produce craters and chains of craters in the surfaces. Finally, the pulsed heat flux of a tokamak leads to thermal fatigue.

Disruptions and run-away electrons cause considerable stresses in the material due to the thermal shock loads, which may lead to cracks. Moreover, the material melts and evaporates in the region of high thermal load. Erosion and evaporation transport material of the first-wall into the plasma. This material is redeposited on first-wall components in the form of droplets of thin layers. In the following some of the plasma induced material damage in plasma facing metallic and ceramic components will be shown.

The behaviour of potential materials for the first wall of fusion reactors, especially for highly stressed components, must be investigated under simulated service conditions. This means that tests must be developed which produce the energy deposition per unit area actually expected, with regard to both the power density and the exposure time or pulse duration. In order to carry out these investigations in the laboratory, the effective and highly complex load histogram has to be split up into single processes. The chemical analysis of the material surface exposed in multiple-shot experiments permits an assessment of the erosion behaviour of a material. In the case of non-destructive testing, for example, a scanning electron microscope (SEM) coupled to an energy-dispersive X-ray analysis (EDAX) system and an image analysis system (IBAS) has been used. The same specimen can be analysed after several beam pulses and then be placed again into the electron beam facility. The eroded material can be chemically analysed using a cooled or uncooled collector probe over the exposed specimen location. In the ideal case, the results of these measurements, which must be carried out by means of Auger electron spectroscopy (AES) because of the thin layer deposited on the collector, should be complimentary to the results obtained for the specimen surface.

6.2.1 Electron, ion and laser beam tests

As mentioned above, in all plasma machine today low Z materials, e.g. fine-grained graphites, different types of carbon-fibre composites, SiC boron containing compounds and refractory metal/graphite composites are used for first-wall components. In addition to the TEXTOR machine experiments, the performance of a material under conditions relevant to fusion is therefore tested in high heat flux electron, ion and laser beam test facilities. The plasma facing components will be subjected to heat fluxes of up to several MWm^{-2} during normal operation: on the other hand, off-normal events have to be taken into account. During these disruptions in the future confinements (e.g. ITER) the deposited peak energy density will be in a range from 2 to 20 $MJ\ m^{-2}$ in a time scale from 0,1 to 3 ms (thermal quench). SEM micrographs of multidirectional CFC after electron and laser beam bonbardment (peak heat flux: 1200 $MW\ m^{-2}$, pulse length: 5 ms, peak energy density: 6 $MJ\ m^{-2}$). Besides thermal erosion the formation of short cracks was found in the matrix of carbon-carbon composites or between the individual filaments in a yarn. Obviously the fibres remain intact, i.e. integrity and thermal conductivity of these materials will not be influenced. The morphology of the eroded surfaces was almost identical in electron and laser beam tests. Differences, however, were observed for the two heat loading methods on the FMI-3-3-3-3 material. During electron beam bombardment the carbon fibres are eroded preferentially, while the laser beam attack shows a relatively homogeneous erosion of fibre and matrix[23].

The thermomechanical performance of SiC coat-mix materials was evaluated in electron and ion beam devices. Main emphasis was laid on the quantification of the thermal shock resistance, for which the specimens were bombarded with 150 keV electrons with different heat load conditions.

Figure 18 show results of electron beam high heat flux tests on SiC coat-mix material. The bombarded surface area was investigated using scanning electron microscopy). Transverse sections were prepared for the determination of erosion depth and material modifications). During these tests the surface temperature was measured by a two-colour pyrometer (Figure 18). The thermal shock resistance of this specially developed coat-mix material was found to be superior to that of other conventional monolithic SiC ceramics. The typical material damages result in the dissociation of SiC and subsequent evaporation of Si and C forming an erosion crater; a fraction of the free silicon diffuses into the bulk where it reacts with the binder coke to form a dense silicon carbide zone. In this region microcracks are initiated due to a mismatch in the thermal expansion coefficients.

6.2.2 Layers in the boronized and carbonized TEXTOR Tokamak

A major prerequisite for operation of present-day Tokamaks under conditions relevant to thermonuclear fusion is that the confined hydrogen plasma is almost free of impurities. A ratio of $<10^{-2}$ of carbon or oxygen to the hydrogen can be tolerated in a plasma, the metal concentration has to be close to 10^{-5}. The impurities in the plasma of Tokamaks with unconditioned metals are surface oxides and carbon compounds of Fe, Ni and Cr. Reducing the impurities is possible by carbonization or boronization, a new type of wall conditioning[24-26]. All plasma facing surfaces were in situ plasma-chemically coated by amorphous boron-doped hydrogenated carbon layer (a-C/B:H) or with an amorphous and hydrogen-rich carbon layer (a-C:H) by using the rf supported glow discharge procedure in a mixture of B_2H_6–H_2 and CH_4–H_2 respectively. The depth composition of the deposited layers have been investigated after the in situ coating steps in TEXTOR by Auger electron spectroscopy combined with Ar sputtering, and by SNMS. As an example, Figure 19 shows an element depth profile of boronized graphite substrate (representative of limiters). Hydrogen, which is indeterminable by AES, is not considered in this distribution. A very broad interface and a significant amount of B (~ 4 at %) deep inside the bulk is featured in the depth profile. The roughness of the graphite surface certainly contributes to the interface broadening. The possibility that molecular B2H6 penetrates during film deposition into pores and reacts there chemically with carbon must also be considered.

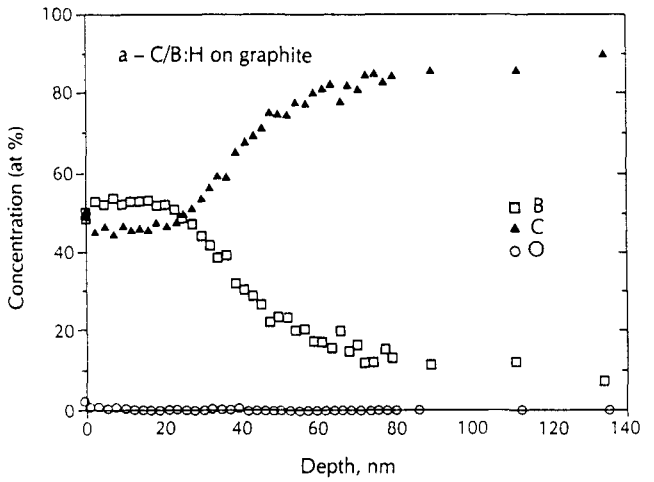

Fig. 19. AES depth profile of boronized graphite[25]

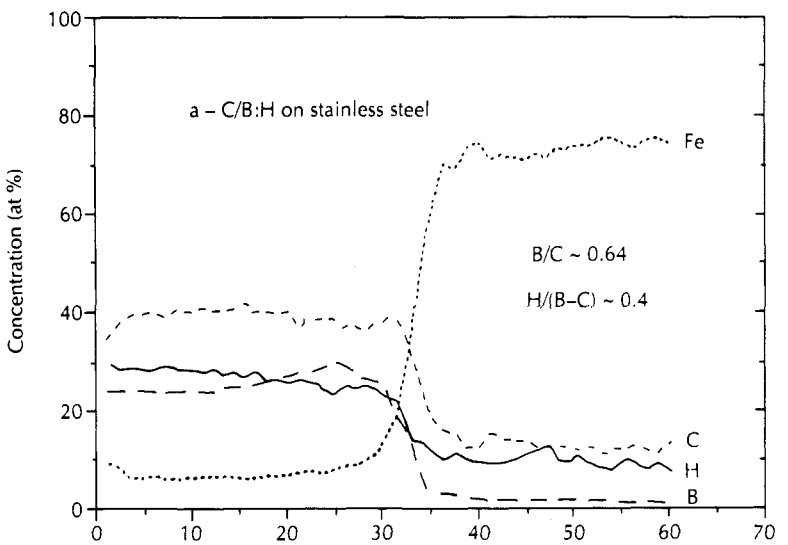

Fig. 20. SNMS depth profile of the a-C/B:H film deposited of stainless steel [26]

The depth distribution of hydrogen in a a-C/B:H was determined by SNMS (Figure 20). A boronized stainless steel (ss) target has been used for this purpose. The constant ratio of H/(B+C) ~ 0,2 across the coating indicates homogeneous hydrogen incorporation.

It has been demonstrated that films deposited on Si, ss, and graphite show rather homogeneous distributions of B, C and H. The boronized layers on the liners of TEXTOR are almost resistant to plasma discharges.

REFERENCES

1. W, Häfeke; Umschau 79, 629 (1979).
2. G. Beckmann and B. Klopries; Fa. Hüls AG, Auszug aus 'Der Lichtbogen', Nr. 208.
3. The first global revolution — a report by the Club of Rome, by Alexander King and Bertrand Schneider, ISBN 0-671-71094-X (1992).
4. G. Lehner and K. Honstatter; Solartechnik (Ullmanns Enzyklopädie der technischen Chemie, Bd. 21), Verlag Chemie, Weinheim, p. 575 (1982).
5. R. Bauer; Fresenius' Z. Anal. Chem. 319, 758 (1984).
6. K.H. Müller; Phys. Bl. 45, A-828 (1989).
7. H. Nickel; Analytical Chemistry in the Exploration, Mining and Processing of Materials, Ed. L.P.R. Butler, p. 181. Blackwell Scientific Publications, Oxford (1986).
8. H. Nickel; Spectrochem. Acta 47B, 27 (1992).
9. H.B. Grübmeier, A. Naoumidis and H.A. Schulze; J. Vac. Sci. Techol. A4, 2665 (1986).
10. H. Nickel, H. Grübmeier, D. Guntur, M. Mazurkiewicz and A. Naoumidis; Fresenius' J. Anal. Chem. 341, 421 (1991).
11. R. Jede, H. Peters, I. Dünnebier, U. Kaiser, S. Meier and O. Ganschow; Techn. Messen 53, 407 (1986).
12. K. Suzuki, T. Ohtsubo, T. Watanabe; Nippon Steel Techn. Report 33, 36 (1987).
13. W.J. Quadakkers; Werkstoffe und Korrosion 41, 659 (1990).
14. W.J. Quadakkers, H. Holzbrecher, K.J. Briefs and H. Beske; Oxidation of Metals 32, 67 (1989).
15. H. Beske, W.J. Quadakkers, H. Holzbrecher, H. Schuster and H. Nickel; Mikrochim. Acta [Wien] II, 109 (1990).
16. C.M. Cotell, K. Przybylski and G.J. Yurek; J. Electrochem. Soc. 116C, Eds. D.A. Shores, G.J. Yurek, Electrochem. Soc. Pennington NJ, p. 103 (1986).
17. H. Cohrt and G. Gratwohl, VDI-Berichte 600.4, 137 (1987).
18. R. Förthmann and A. Naoumidis, Werkstoffe und Korrosion 41, 728 (1990).
19. M. Reisch, H. Nickel and M. Mazurkiewics; Spectrochim. Acta 44B, 307 (1989).
20. H. Nickel, M. Reisch and M. Mazurkiewicz; Fresenius Z. Anal. Chem. 335, 631 (1989).
21. H. Nickel, Z. Zadgorska and G. Wolff; Spectrochem. Acta (in press).
22. J. Eidens and H. Wolf; Atomwirtschaft/Atomtechnik 138, XXVII (1982).
23. J. Linke, H. Hoven, K. Koizlik and H. Nickel; High-temp. High Pressure 21, 533 (1989).
24. J. Winter; J. Nucl. Mat. 161, 265 (1989).
25. J.V. Seggern, H. Peters, H.G. Esser, P. Wienhold and J. Winter; Vacuum 41, 1486 (1990).
26. T. Banno, P. Wienhold, J. Winter and F.G. Waekbroeck; Vacuum 41, 1489 (1990).